NASA Technical Memorandum 102024

Parametric Study of Electromagnetic Waves Propagating in Absorbing Curved S Ducts

Kenneth J. Baumeister
Lewis Research Center
Cleveland, Ohio

July 1989

NASA

PARAMETRIC STUDY OF ELECTROMAGNETIC WAVES PROPAGATING IN ABSORBING CURVED S-DUCTS

Kenneth J. Baumeister
National Aeronautics and Space Administration
Lewis Research Center
Cleveland, Ohio 44135

SUMMARY

A finite-element Galerkin formulation has been developed to study attenuation of transverse magnetic (TM) waves propagating in two-dimensional S-curved ducts with absorbing walls. In the frequency range where the duct diameter and electromagnetic wave length are nearly equal, the effect of duct length, curvature (duct offset), and absorber wall thickness was examined. For a given offset in the curved duct, the length of the S-duct was found to significantly affect both the absorptive and reflective characteristics of the duct. For a straight and a curved duct with perfect electric conductor terminations, power attenuation contours were examined to determine electromagnetic wall properties associated with maximum input signal absorption. Offset of the S-duct was found to significantly affect the value of the wall permittivity associated with the optimal attenuation of the incident electromagnetic wave.

E-4761

INTRODUCTION

Electromagnetic propagation in curved ducts (wave guides) plays an important role in many practical physical systems. In microwave power generation systems, for example (Kennedy, 1985, pp. 315-317), bends or corners are required to alter the direction of the wave. Since curves or corners represent discontinuities, reflection from bends can be significant. Recent work (Burkholder, 1987 and Chou, 1987) has been concerned with the absorption of electromagnetic waves in curved ducts.

In the present paper, a finite-element Galerkin formulation has been developed to study wave propagation in curved S-shaped ducts with absorbing walls. Figure 1 illustrates the various processes of reflection and absorption which can occur when electromagnetic energy flows into a curved duct. This paper will focus on the interaction of a propagating duct mode traveling down the uniform entrance duct with the curved walls as shown in figure 1. The reflection and transmission at the entrance and exit of the curved duct are determined by coupling the finite-element solutions in the curved duct to the eigenfunctions of the infinite, uniform, perfectly conducting entrance and exit ducts. This permits a multimodal representation accounting for reflection and mode conversion by the nonuniform curved section.

In a number of parametric studies, the effect of duct length, curvature (duct offset), and wall thickness are examined. In addition, for a PEC (perfect electrically conducting) termination, a computational search is used to determine the wall properties which lead to a local maximum attenuation of the incident electromagnetic wave for both a straight and curved S-duct.

NOMENCLATURE

A	property term, equation (20)
B	property term, equation (21)
A_n^+	mode amplitude of positive going entrance waves, equation (8)
A_n^-	mode amplitude of reflected negative going entrance wave, equation (8)
B_n^+	mode amplitude of positive going exit waves, equation (11)
b'	characteristic duct height
b_a	dimensionless entrance height b_a'/b'
b_b	dimensionless exit height b_b'/b'
c_o'	speed of light in vacuum
f	dimensionless frequency, equation (7)
H_x	x component of magnetic intensity, H_x'/H_o'
H_o'	normalizing magnitude of magnetic intensity
$\tilde{H}_x$	finite-element approximation to H_x
j	$\sqrt{-1}$
k	wave number
k_{zn}	axial modal wave number, equations (9) and (10)
L	dimensionless length, L'/b_a'
m	mode number, equation (13)
N_m	number of modes in expansion, equation (13)
P_o	power of positive going entrance wave
P_x	power in axial direction
T	dimensionless thickness of absorber wall
t	dimensionless time, $\frac{c_o'}{b_a'} t'$

x dimensional transverse distance, x'/b_a'

y dimensionless transverse distance, y'/b_a'

z dimensionless axial distance, z'/b_a'

ε total complex permittivity, equation (4)

ε' permittivity

ε_a dielectric constant in entrance duct, $\varepsilon_a'/\varepsilon_o'$

ε_o' permittivity in vacuum

ε_r complex dielectric constant, $\varepsilon'/\varepsilon_o'$

ε_r^I imaginary part of dielectric constant

ε_r^R real part of dielectric constant

ε_T^I total imaginary part of permittivity, equation (4)

η intrinsic impedance

λ wavelength

μ total permeability, equation (5)

μ' permeability

μ_o' permeability in vacuum

μ_r relative permeability, μ/μ_o'

μ_r^I imaginary part of relative permeability

μ_r^R real part of relative permeability

σ dimensionless conductance, $\dfrac{\sigma' b_a'}{c_o' \varepsilon_o'}$

ω dimensionless angular velocity, $\dfrac{\omega' b_a'}{c_o'}$

ω' angular velocity

Subscripts

a entrance region

b exit region

Superscripts

' dimensional quantity

~ approximate quantity

GEOMETRIC MODEL

In the finite-element modeling, an S-shaped profile has been chosen to approximate the two-dimensional cross-sectional profile that might be found in a typical bend, as shown in figure 2. The S-shaped profile can be prescribed by a simple third-degree polynomial of the form

$$y = h\left[3\left(\frac{z}{L}\right)^2 - 2\left(\frac{z}{L}\right)^3\right] \tag{1}$$

where the dimensionless duct coordinates are defined as

$$y = \frac{y'}{b_a'} \qquad z = \frac{z'}{b_a'} \qquad L = \frac{L'}{b_a'} \tag{2}$$

and b_a' is the height of the straight duct leading into the curved duct and h is the offset height of the duct. The S-curve defined by equation (1) has zero slope at z/L of 0 and 1; providing a smooth transition from a straight entrance to the curved test section. In the foregoing equations, the prime, ', is used to denote a dimensional quantity and the unprimed symbols define a dimensionless quantity. This convention will be used throughout this report. These and all other symbols used in the report are defined in the nomenclature.

GOVERNING EQUATION

For time harmonic ($e^{+j\omega t}$) variations in the electromagnetic field, the governing differential equations are the standard Maxwell's equations which can be combined to form a single variable property wave equation for the transverse magnetic wave propagation (Silvester, 1983, pg. 48, eq. 4.07). For a two-dimensional duct, the scalar form of the wave equation can be written as (Baumeister, 1988, eq. 13)

$$\frac{\delta}{\delta y}\left(\frac{1}{\varepsilon}\frac{\delta H_x}{\delta y}\right) + \frac{\delta}{\delta z}\left(\frac{1}{\varepsilon}\frac{\delta H_x}{\delta z}\right) + \omega^2 \mu H_x = 0 \tag{3}$$

where the total permittivity including conduction (Cheng, pg. 300 or Harrington, pp. 24 and 25, eq. (1-74) and (1-76)) and the total permeability (Harrington, pg. 25, eq. (1-77)) are defined as

$$\varepsilon = \varepsilon_r^R - j\left(e_r^I + \frac{\sigma}{\omega}\right) = \varepsilon_r^R - j\,\varepsilon_T^I \tag{4}$$

$$\mu = \mu_r^R - j\mu_r^I \tag{5}$$

the various parameters are real positive quantities with

$$\sigma = \frac{\sigma' b_a'}{c_o' \varepsilon_o'} \tag{6}$$

and the dimensionless frequency f is defined as

$$f = \frac{f' b_a'}{c_o'} = \frac{b_a'}{\lambda_o'} \qquad \omega = 2\pi f \tag{7}$$

Because of computer storage limitations, the present finite element formulation will be restricted to structures where the duct height is the same order of magnitude as the wavelength.

UNIFORM DUCT ANALYTICAL SOLUTIONS

The analytical solutions of equation (3) for wave propagation in the uniform perfectly conducting duct having an anechoic entrance and exit will be employed to give the proper termination boundary condition for the finite-element region. The analytical solution of equation (3) for TM waves traveling between perfectly conducting parallel plates is given as (Cheng, 1983, pg. 458):

$$H_{xa} = \sum_{n=1}^{N_m} A_n^+ \cos\left(\frac{(n-1)\pi y}{b_a}\right) e^{-jk_{zn}z} + \sum_{n=1}^{N_m} A_n^- \cos\left(\frac{(n-1)\pi y}{b_a}\right) e^{+jk_{zn}z} \tag{8}$$

For the $e^{+j\omega t}$ time dependence used here, the A_n^+ represents a wave propagating in the positive z direction while A_n^- term represents a wave moving in the negative z direction

The axial wave number k_{zn} in equation (8) is

$$k_{zn} = +k \quad 1 - \left(\frac{(n-1)\pi}{b_a k}\right)^2 \quad \left(\frac{(n-1)\pi}{b_a k}\right) \leq 1 \tag{9}$$

$$k_{zn} = -jk \quad \left(\frac{(n-1)\pi}{b_a k}\right)^2 - 1 \quad \left(\frac{(n-1)\pi}{b_a k}\right) > 1 \tag{10}$$

A similar solution exists at the exit, except only positive going waves are considered

$$H_{xb} = \sum_{n=1}^{N_m} B_n^+ \cos\left(\frac{(n-1)\pi y}{b_b}\right) e^{-jk_{zn}z} \tag{11}$$

BOUNDARY CONDITIONS

A variety of boundary conditions will be used in the finite-element solution of equation (3) for the model problems which are displayed in schematic form in figures 3 and 4. Each of the required conditions will now be briefly discussed.

Input Conditions

The analysis assumes a given number N_m of propagating A_n^+ modes (eq. 8). These modes effectively set the level of the magnetic field in the finite element region and can be viewed as the equivalent Dirichlet boundary condition required for the elliptic boundary value problem as defined by equation (3).

The modal expression represented by equation (8) has been truncated to a total of N_m modes of the infinite number possible. Thus, a total of N_m unknown modal amplitudes A_1^-, A_2^-, . . . A_{Nm}^- have been introduced. N_m constraint equations will be required to determine each of these unknown reflection coefficients. The equations used to determine these coefficients will now be introduced.

Continuity at Inlet and Exit

The tangential component of an H field is continuous across an interface between two physical real media which are not perfect conductors (Kraichman, 1970, eq. (1.61)). Thus, the boundary condition becomes

$$H_{xa} = \tilde{H}_x \quad (z = 0;\ 0 \geq y \leq b_a) \tag{12}$$

where H_{xa} is the modal representation of the magnetic field in the analytical inlet region given by equation (8) and $\tilde{H}_x$ represents the finite-element numerical solution to be discussed in detail in a following section of this report.

At the inlet to the curved section, shown in figures 3 or 4, the H_{xa} in the analytical region given by equation (8) must match the magnetic field defined by the finite-element nodal points along the boundary interface. Many possible mode matching schemes can be employed for this boundary condition, such as point collocation, least squares, or weighted residuals. A weighted residual approach was used herein with the weighting function equal to the eigenfunctions for the uniform infinitely long duct with perfectly conducting walls;

$$\int_0^{b_a} \left[H_{xa}(y) - \tilde{H}(y)\right] \cos\left(\frac{(m-1)\pi y}{b_a}\right) dy = 0 \qquad \text{at} \quad z = 0 \tag{13}$$

(N_m equations, $m = 1, 2, 3, \ldots N_m$)

Equation (13) represents N_m separate equations; one for each coefficient defined in equation (8). The symbol m has been introduced as a dummy variable to make it distinct from the multiple n mode numbers that make up the H_{xa} analytical function. A similar situation exits at the exit.

In addition to the tangential component of the magnetic field, the tangential component of the electric field must also be continuous across the interface (Cheng, 1983, eq. (7-52(a))). Using Maxwell's equations to express the tangential electric field in terms of the magnetic field (Jordan, 1968, eq. (7-4)) yields

$$\frac{1}{\varepsilon} \frac{\delta \tilde{H}_x}{\delta z} = \frac{1}{\varepsilon_a} \frac{\delta H_{xa}}{\delta z} \tag{14}$$

Perfectly Conducting Wall Conditions

At a perfectly conducting wall surrounding the duct or at the exit plane in figure 4, the tangential component of the electric field vector is zero (Cheng, 1983, eq. (7-52(a)) or Kraichman, 1970, eq. (1.69)). Again, using Maxwell's equations to relate the electric field to the magnetic field (Jordan, 1968, eq. (7-4)), the component of the gradient of the magnetic filed normal to a perfectly conducting wall becomes

$$\nabla \tilde{H_x} \cdot \bar{n} = 0 \tag{15}$$

FINITE ELEMENT THEORY

The finite element weak formulation of the wave equation (3) is now generated by using the weighted residual approach with the Galerkin approximation. The continuous domain D is first divided into a number of discrete triangular areas as shown in figure 5. The finite element aspects of converting equation (3) and the boundary conditions into an appropriate set of global difference equations can be found in text books (Burnett, 1987, pp. 561-564) and for conciseness will not be presented herein. An exact adaption of this standard finite element theory to the duct propagation problem can be found in an earlier work (Baumeister, 1988).

RESULTS AND COMPARISONS

A number of example calculations are now presented to illustrate the use of the code as applied to curved ducts with absorbing walls. First, typical duct geometries and element arrangements used in the numerical examples are discussed. Next, the effect of offset and duct length on the transmitted and reflected energy are examined for a fixed wall absorption layer. Then, the effect of absorber thickness is considered. Finally, for a PEC exit termination, the power attenuation contours for a curved and straight duct which maximize input signal absorption are examined.

Duct Geometry

The grid generation package generates the geometries shown in figure 6, where a typical straight duct and curved duct with maximum offset (h = 1) are shown. The absorber has been placed above and below the duct. All the duct geometries are of this form but with different lengths, offsets and absorber thickness. The linear triangular finite element grid associated with this geometry is shown in figure 7.

Example 1: Transmitted Power

The effect of duct curvature and length on transmitted power in an infinite duct are examined in figure 8 for various values of duct offset. The geometrical configuration is shown by the inserted sketch in figure 8. In this case, the entrance and exit ducts stretch from minus infinity to plus infinity which signifies the absence of reflected energy at the numerical terminations. The wall properties were taken to be $\varepsilon_w = 1.00-2.83j$ and $\mu_w = 4$. These properties are associated with nearly maximum absorption of a plane TM wave in a straight duct at the frequency of unity. For a fixed length of duct, as seen in figures 8(a), (b), and (c), an increase in the duct offset parameter h increases the attenuation of the transmitted electromagnetic power (Poynting vector, cross product of the electric and magnetic fields times duct area, Baumeister 1988 pg. 23 or Cheng 1983, pg. 330) at the exit of the curved lined portion. This effect is most pronounced for the smaller duct lengths as shown in figures 8(a) and (b). The magnetic intensity fields inside the duct are illustrated in figure 9 for the duct with 0.75 length. As seen in figure 9(a) the magnetic intensity beams directly through the duct with grazing contact along the absorbing wall till it reaches the exit with very little

attenuation. In contrast, in figure 9(e) the magnetic field comes in nearly normal contact with the wall and quickly dies out. Returning to figure 8(a), note that the dimensionless power drops below the input value of 1 for large values of the offset parameter h. This signifies increased reflection of the curved portion of the duct. This reflection will now be examined.

Example 2: Reflected Power

The effect of duct curvature and length on the reflected power from the curved portion of a semi-infinite duct are now examined in figure 10 for various values of duct offset. Again, the geometrical configuration is shown by the inserted sketch in figure 10. To highlight the reflected energy in example in figure 10, the termination at the exit is a PEC (perfect electric conductor) plate which reflects all the energy which reaches the exit back towards the infinitely long entrance duct.

For a fixed duct length, as seen in figure 10, increasing the liner offset h generally decreases the reflection coefficient. However, for ducts with lengths of 0.75 and 1.0, an optimum is reached. In these cases, the discontinuity of the curvature appears to reflect significant energy back down the duct before it can be absorbed. Figure 11 shows the magnetic fields inside with the length of 0.75. For the straight duct the interaction of the field is clearly seen in figure 11(a). In contrast, the field in the duct with large offset ($h = 1$) are comparable to those in figure 9(e), because the level has been severely reduced by absorption into the duct walls.

Example 3: Absorber Thickness

In this section the effect of absorber thickness is briefly examined. The configuration considered is again shown by the sketch in the upper portion of figure 12. In this case the duct length and offset will be held fixed at unity and the wall absorber thickness will be varied. As seen in figure 12 for thickness of 0.1 or greater, the power variation along the axial length of the duct remains unchanged. However, for thickness of 0.05 and 0.01 significant decreases in the power absorbed are seen.

Example 4: Axial Discretization in Wall Absorber

In performing finite element solutions, the number of axial nodal points should be held to a minimum to reduce computer storage as well as solution time. This is especially true in the next example where determining the wall properties associated with optimum signal absorption requires hundreds of separate calculations starting with large values of wall permittivity and permeability.

For linear elements, roughly twelve grid points per wavelength are required to accurately resolve the complex electromagnetic field and the transmitted or reflected electromagnetic power. The wave length for plane wave propagation in lossy material will now be determined from a solution of the wave equation. For plane waves propagating in a homogeneous lossy material, equation (3) reduces to

$$\frac{\delta}{\delta z}\left(\frac{\delta H_x}{\delta z}\right) + \omega^2 \varepsilon \mu H_x = 0 \tag{16}$$

The solution of which can be written as

$$H_x = H_o\, e^{-\alpha z}\, e^{-j\beta z} \tag{17}$$

where

$$\alpha = \frac{\omega}{2}\left[\sqrt{A^2 + B^2} - B\right]^{1/2} \tag{18}$$

$$\beta = \frac{\omega}{2}\left[\sqrt{A^2 + B^2} + B\right]^{1/2} \tag{19}$$

$$A = \varepsilon_T^I \mu_r^R + \varepsilon_r^R \mu_r^I \tag{20}$$

$$B = \varepsilon_T^R \mu_r^R - \varepsilon_r^I \mu_r^I \tag{21}$$

and the wavelength can be expressed in terms of the propagation phase constant β as follows:

$$\lambda = \frac{2\pi}{\beta} \tag{22}$$

The number of grid points I in the axial direction to accurately resolve the electromagnetic field is

$$I = 12\,\frac{L}{\lambda} = \frac{6\beta L}{\pi} \tag{23}$$

For the special case where the duct length is just equal to the axial wavelength of the electromagnetic wave, twelve nodal points are required in the axial direction. If the duct length is twice the wavelength then 24 nodes would be required. Thus the number of nodes is just 12 times the duct length to wavelength ratio.

For large values of the permittivity and permeability associated with wall absorbers, the phase constant β increases according to equation (19) which leads to smaller values of the wavelength according to equation (22) and a considerably larger number of axial nodes according to equation (23). However, a plane wave incident obliquely at an interface with a denser medium will be bent toward the normal (Cheng, 1983, pg. 353, eq. 8-124(c)) making the

energy transfer in the wall absorber normal to the direction of the energy transfer in the duct itself and thereby partially reducing the axial energy transfer in the wall absorber. Since the axial attenuation in the duct wall will be much larger than in the air duct, consideration is now given to basing the axial grid spacing on the wavelength of the air duct rather than the wall absorber wave length. In this case the axial grid point spacing would be

$$I = 12 \frac{L}{\lambda_{air}} = 12\ Lf \qquad (\text{eq. } 19)\beta = \omega\sqrt{\varepsilon_T^R \mu_r^R} = \omega = 2\pi f) \qquad (24)$$

If such an approximation is valid, larger savings in computer storage are possible.

The validity of equation (24) in predicting energy attenuations and magnetic fields is now examined for two extremes of wall properties. First the moderate value listed in figure 13(a) and the much larger value listed in figure 13(b). As seen in the upper portion of figure 13(a), axial spacing based on the wall properties using equation (23) results in a much denser grid than the lower figure based on the wavelength in air using equation (24). For the large wall property value, the grid density is even greater as seen in the upper portion of figure 13(b). For the duct configuration shown in the upper portion of figure 14, exact calculations for duct attenuation displayed in figure 14 indicate that the axial spacing based on air properties, equation (24) gives nearly the same results as the axial spacing based on the wall material, equation (23). In addition, the contour plots of the magnetic field shown in figure 15(a) and (b) show that the magnetic field in the duct is for all practical purposes identical when either equation (23) or (24) is employed to set the axial grid point density. Therefore, in the next optimization example, equation (24) will be used to set the axial grid spacing.

Finally, the sensitivity to the number of transverse nodes in the wall absorber is determined in figure 16. As seen in figure 16 at least 5 nodes are required to accurately estimate the attenuation in a 0.1 thick absorber coating with the same range of property variations previously considered.

Example 5: Attenuation Contours

Optimizing the wall absorber for maximum attenuation as well as minimizing duct reflection can be an important part of the design of an electromagnetic duct suppressor. In duct acoustics, for example, the maximum possible attenuation occurs at the so-called optimum impedance. For a particular acoustic mode (analogous to an electromagnetic mode) or more generally for modes with common cut-off ratios, the optimum impedance can be determined analytically from semi-infinite duct theory using a single soft-wall mode (Rice, 1979). Generally, the optimum impedance for a finite length liner will be lower than the single mode liner due to generation of higher order modes at the leading edge of the finite length liner (Unruh, 1976 and Baumeister, 1984).

Since electromagnetic propagation and attenuation is analogous to acoustic propagation, an electromagnetic wall impedance should exist which can be expected to maximize absorption by the duct wall absorbers. However, in the present computer code, the wall properties are specified rather than wall

impedance. Consequently, the local attenuation optimum will be determined for specific values of wall properties rather than the more general global optimum analogous to Rice, 1979.

Consider a plane wave propagating down a duct and incident upon the curved section with a PEC exit plane, as shown in the schematic of figure 17. The object of the present example is to estimate the wall properties which will minimize the reflected signal transmitted back down the duct or conversely to maximize the energy absorbed by the wall absorber. Starting with a single plane wave traveling down the duct and initially assuming a wall permeability of 4.1 in the curved absorber section of the duct, the reflected energy was determined throughout the permittivity plane shown in figure 17. With increments of 0.5 taken in the real and imaginary parts of the permittivity, 400 separate calculations were performed at the equally spaced nodes. From these calculations, the attenuation contour plots were established using inear interpolation between the calculated points.

The local optimum wall value of the permittivity is seen in figure 17 to occur at a total permittivity of 5.0 - j 5.0. The coordinates of figure 17(a) are the real positive values of both ε_r^R and ε_T^I defined in equation (4). In this case, the optimum wall permittivity associated with maximum signal absorption is represented by the peak contours enclosed in the smallest circle of figure 17(a). For this first iteration, the intrinsic (or characteristic) impedance of the material squared is 0.41 + j 0.41 as shown in the upper portion of figure 17(a).

The maximum attenuation of the incoming wave is 23.903 dB associated with the local optimum point as displayed in figure 17(a) where the attenuation in dB is expressed in terms of the transmitted power P_x (Baumeister, 1986, eq. 88) as

$$dB = 10 \log_{10}\left[\frac{P_x}{P_o}\right] \tag{25}$$

The maximum and minimum attenuation in absolute values of dB are listed in figure 17(a) as well as each figure which follows. The dB contours have been normalized in figure 17 as well as the following figures by the simple equation:

$$|dB_{contour}| = \frac{|dB| - |dB_{min}|}{|dB_{max}| - |dB_{min}|} \tag{26}$$

The second step in the iteration process to determine the optimum wall properties is to hold the permittivity fixed and vary the permeability. In this case, the optimum wall value of the permeability is seen in figure 17(b)

to occur at a total permeability of 6.0 - j 8.5. For this second iteration, the intrinsic impedance squared has shifted to 1.45 j 0.25 and the maximum attenuation has increased to 28.73 dB.

The third and final iteration is shown in figure 17(c) in which the optimum value of wall permeability was held fixed at the value of 6.0 - j 8.5 determined during the second iteration. In the third iteration, the optimum properties remained fixed at the values determined during the second iteration indicating a local convergence over the range considered. Figure 17(c) differs from figure 17(a) in that attenuation can now occur for zero values of the complex permittivity since the permeability is now a complex quantity which can contribute to the attenuation of the incoming wave.

For the same geometry as considered in figure 17, the sensitivity of the initial starting point on the electromagnetic reflective energy contours is examined in figure 18. In this case the initially fixed value of permeability is 2.0 rather that 4.1 as used in figure 17(a). A comparison of figure 17(a) to figure 18(a) indicates that the first estimate for the optimum has been shifted to the right in figure 18(a). The optimum in the second iteration falls slightly off the range of parameters considered. However, the maximum attenuation of 27.945 at a permeability of 10 - j 10 and permittivity of 9 - j 5.5 is nearly equal to the optimum attenuation of 28.73 dB displayed in figure 17(c). Apparently, the optimum contours have slowly varying slopes. However, in both cases considered, the intrinsic impedance of the medium are nearly equal. Consequently, it may be inferred that any combination of material properties with a similar intrinsic impedance should yield similar values of attenuation.

Figure 19(a) and (b) displays similar results for the straight duct of the same length as considered in figure 17. In this case the local optimum attenuation has a maximum value of 22.113 dB which is approximately 6 dB lower than the curved duct considered in figures 17 and 18. More significantly, the optimum intrinsic impedance has shifted to a new value of 0.1 + j 0.7. Clearly, the curvature of the duct will play a significant role in determining the wall materials to obtain the maximum attenuation.

CONCLUDING REMARKS

A finite-element Galerkin formulation was developed to study transverse magnetic (TM) wave propagation in two dimensional curved S-shaped ducts with absorbing walls. The derivation from Maxwell's equations assumed that the material properties could vary with position resulting in a nonhomogeneous variable property two-dimensional wave equation. This eliminated the necessity of finding the boundary conditions between the air duct and the absorbing walls. The reflection and transmission at the entrance and exit of the curved duct are determined exactly by coupling the finite-element solutions in the curved duct to the eigen-functions of an infinite, uniform, perfectly conducting duct.

Example solutions illustrated the relationship of absorption on the length, thickness and offset of curved duct absorbing walls. Also, attenuation contour plots were presented for PEC ended curved ducts. Local optimum wall

values of permittivity and permeability as well as the intrinsic impedance associated with the optimum were found to be significantly different for straight and curved ducts with PEC exits.

REFERENCES

1. Baumeister, K.J.: Electromagnetic Propagation in PEC and Absorbing Curved S-Ducts. NASA TM-100833, 1988.

2. Baumeister, K.J.: Finite Element Analysis of Electromagnetic Propagation in an Absorbing Wave Guide. NASA TM-88866, 1986.

3. Baumeister, K.J.; and Horowitz, S.J.: Finite Element-Integral Acoustic Simulation of JT15D Turbofan Engine. J. Vibration, Acoustics Stress, Rel. Design, vol. 106, no. 3, July 1984, pp. 405-413.

4. Burnett, D.S.: Finite Element Analysis. Addison-Wesley, Reading, MA, 1987.

5. Burkholder, R.J.; Chuang, C.W.; and Pathak, P.H.: Electromagnetic Fields Backscattered from an S-Shaped Inlet Cavity with an Absorber Coating on its Inner Walls. (FR-715723-2, Ohio State University; NASA Grant NAG3-476) NASA CR-182401, 1987.

6. Cheng, D.K.: Field and Wave Electromagnetics. Addison-Wesley, 1983.

7. Chou, R.; Ling, H.; and Lee; S.W.: Reduction of the Radar Cross Section of Arbitrarily Shaped Cavity Structures. (UILU-ENG-87-2560, UILU-TR-87-6, University of Illinois at Urbana-Champaign; NASA Grant NAG3-475) NASA CR-180307, 1987.

8. Harrington, R.F.: Time-Harmonic Electromagnetic Fields. McGraw-Hill, 1961.

9. Jordan, E.C.; and Balmain, K.G.: Electromagnetic Waves and Radiating Systems, 2nd ed., Prentice-Hall, 1968.

10. Kraichman, M.B.: Handbook of Electromagnetic Propagation in Conducting Media. NAVMAT P-2302, U.S. Government Printing Office, Washington, D.C., 1970.

11. Kennedy, G.: Electronic Communication Systems, 3rd ed., McGraw-Hill, 1985.

12. Rice, E.J.: Optimum Wall Impedance for Spinning Modes - A Correlation with Mode Cutoff Ratio. J. Aircraft, vol. 16, No. 5, May 1979, pp. 336-343.

13. Silvester, P.P.; and Ferrari, R.L.: Finite Elements For Electrical Engineers. Cambridge University Press, Cambridge, England, 1983.

14. Unruh, J.F.: Finite Length tuning for Low Frequency Lining Design. J. Sound Vibration, vol. 45, no. 1, Mar. 8, 1976, pp. 5-14.

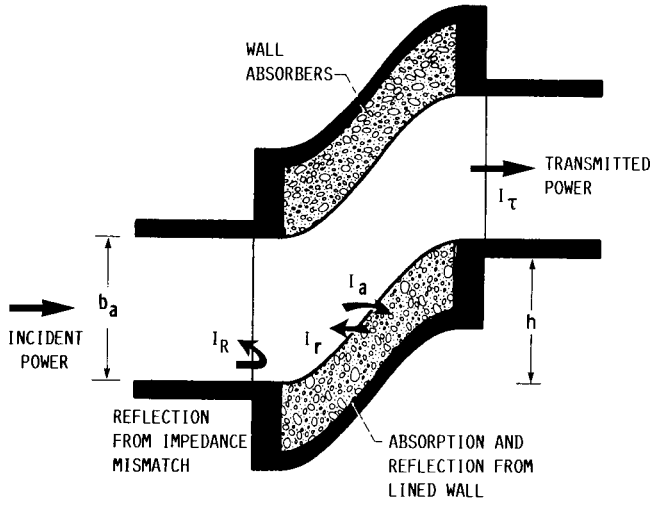

FIGURE 1. - REFLECTIVE AND ABSORPTION CHARACTERISTICS OF LINED S-DUCT.

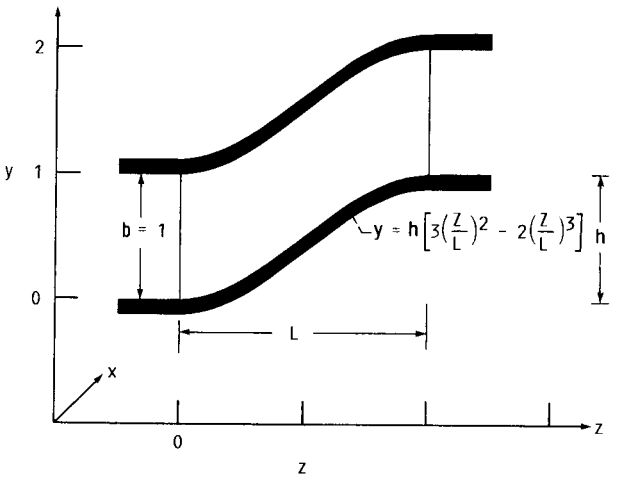

FIGURE 2. - S-DUCT GEOMETRY AND COORDINATE SYSTEM.

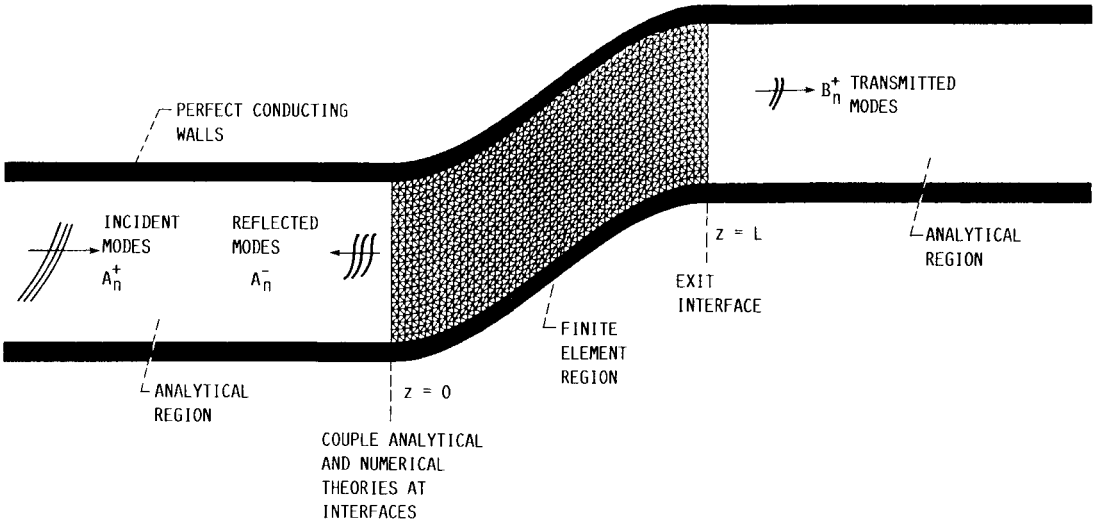

FIGURE 3. - TWO DIMENSIONAL S-DUCT FINITE ELEMENT MODEL.

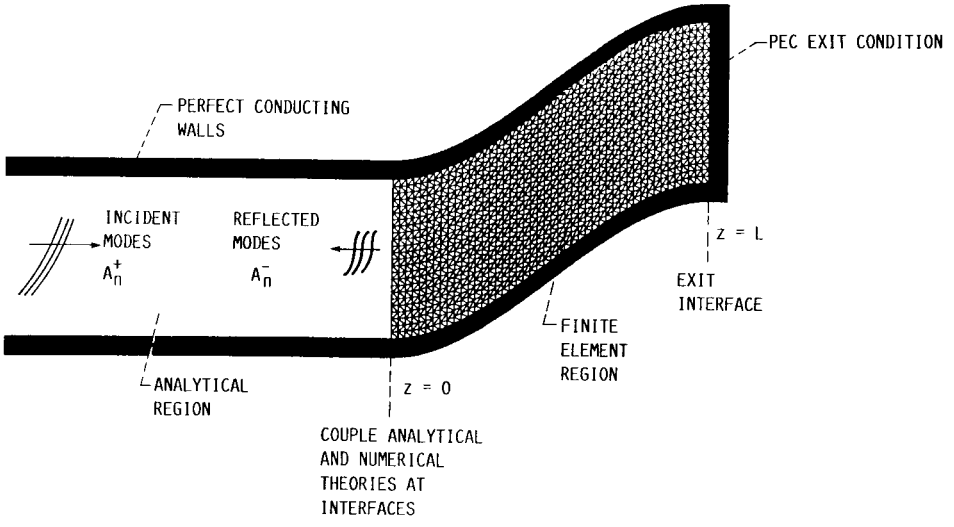

FIGURE 4. - TWO DIMENSIONAL S-DUCT FINITE ELEMENT MODEL WITH PEC EXIT PLANE.

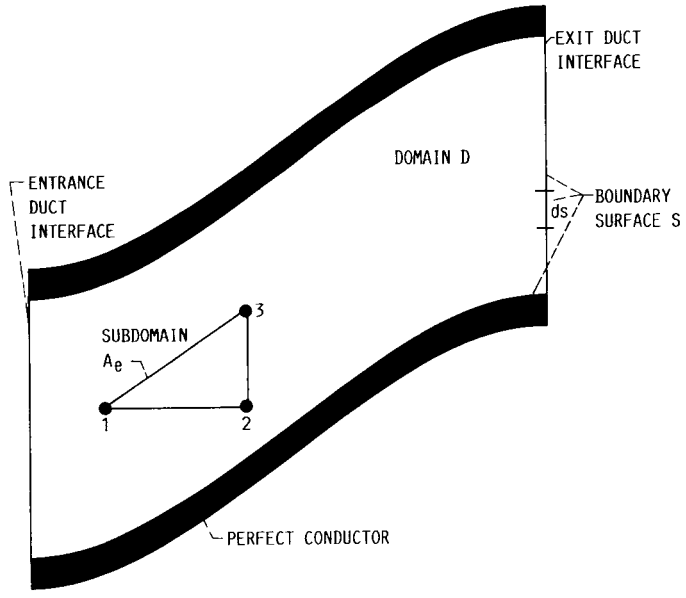

FIGURE 5. - ELECTROMAGNETIC BOUNDARY VALUE FORMULATION.

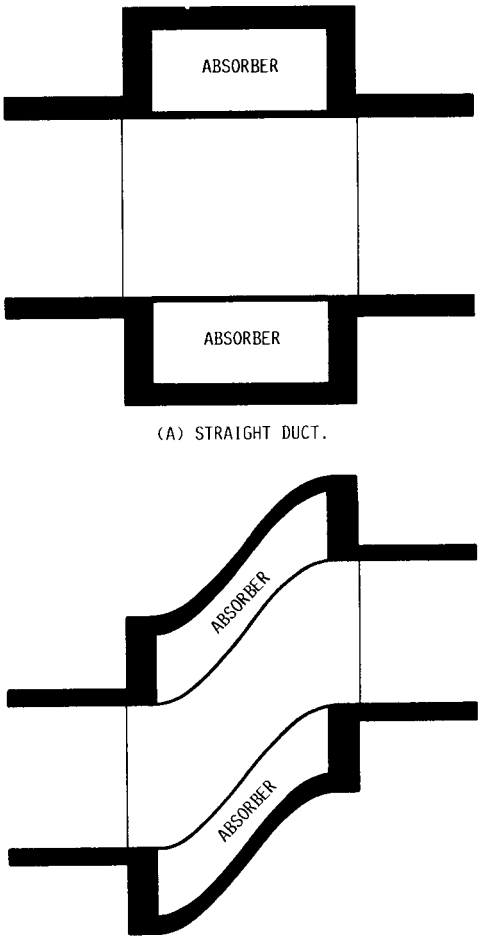

(A) STRAIGHT DUCT.

(B) CURVED DUCT.

FIGURE 6. - ABSORBING WALL DUCT CONFIGURATIONS.

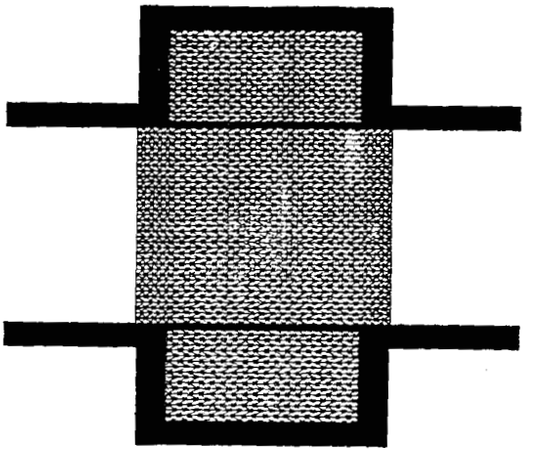

(A) STRAIGHT DUCT.

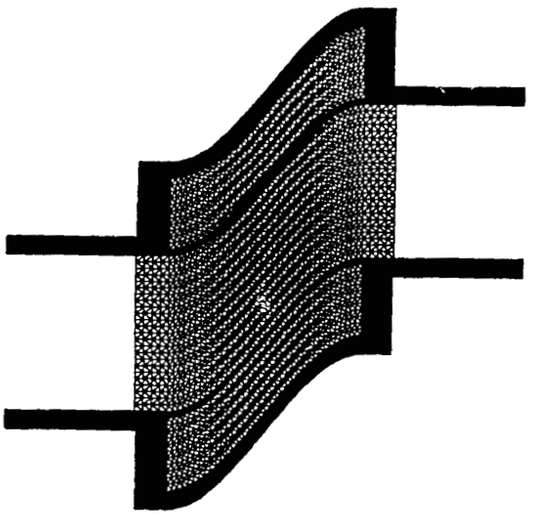

(B) CURVED DUCT.

FIGURE 7. - DISCRETIZATION OF AIR FILLED WAVE GUIDE WITH ABSORBERS MOUNTED ALONG BOTH UPPER AND LOWER WALLS.

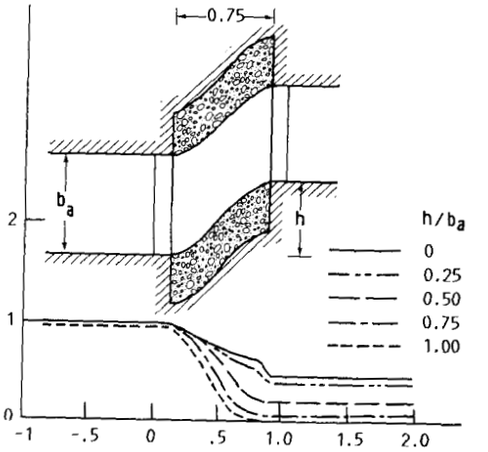

(A) L = 0.75.

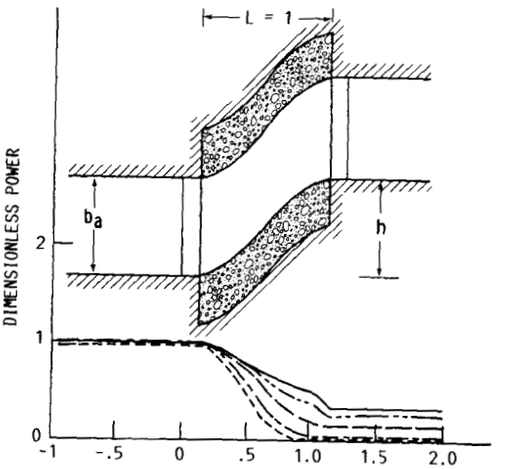

(B) L = 1.0.

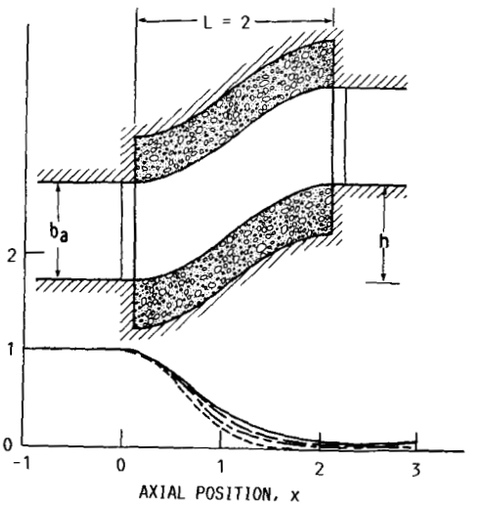

(C) L = 2.

FIGURE 8. - EFFECT OF DUCT OFFSET ON THE MAGNITUDE OF THE AXIAL POWER AS A FUNCTION OF POSITION (WALLS $\varepsilon_\omega = 1. - j2.83$; $\mu_\omega = 4.1$ AND $f = 1$).

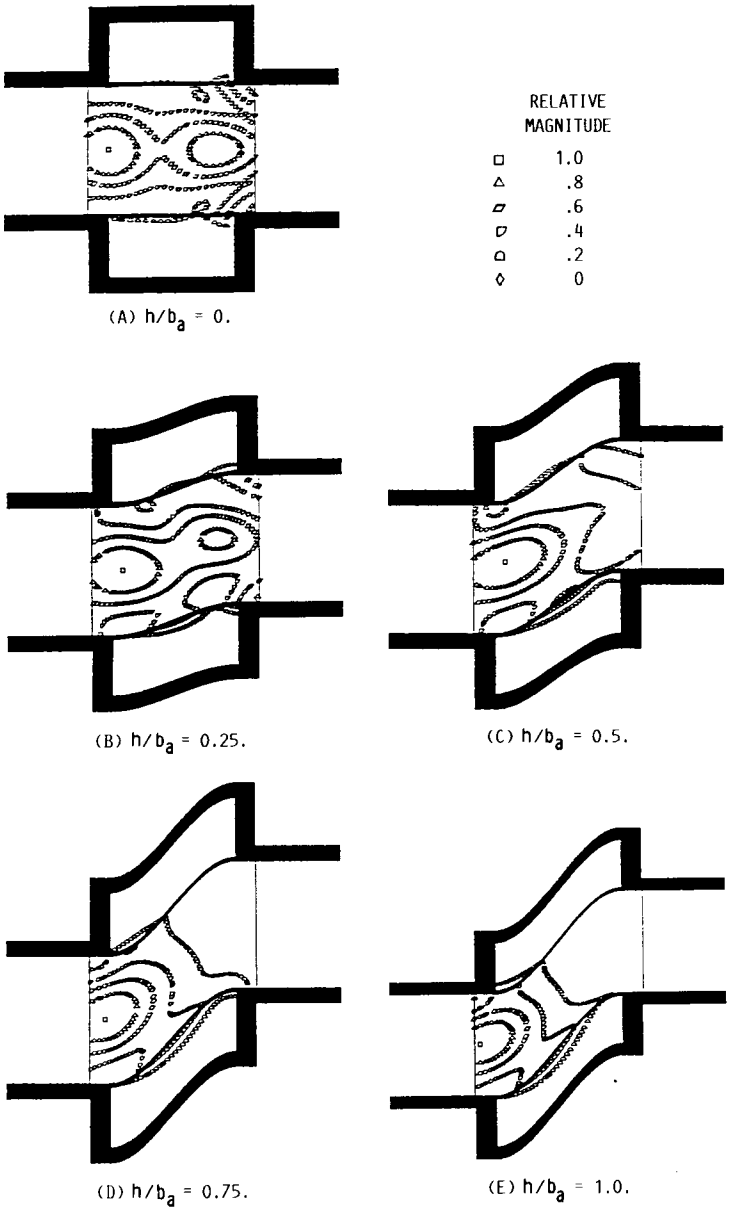

FIGURE 9. - EFFECT OF OFFSET OF ABSORBING WALL ON THE CONTOURS OF THE MAGNETIC FIELD WITH NONREFLECTING EXIT FOR L = 0.75 AND f = 1.

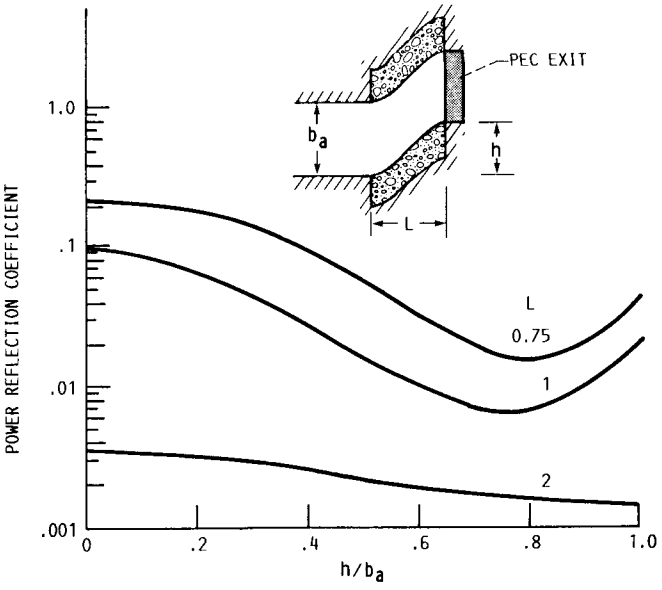

FIGURE 10. - EFFECT OF DUCT OFFSET h ON THE AXIAL POWER REFLECTION COEFFICIENT AS A FUNCTION OF DUCT LENGTH ($\varepsilon_\omega = 1. - j2.83$; $\mu = 4.1$ AND $f = 1$).

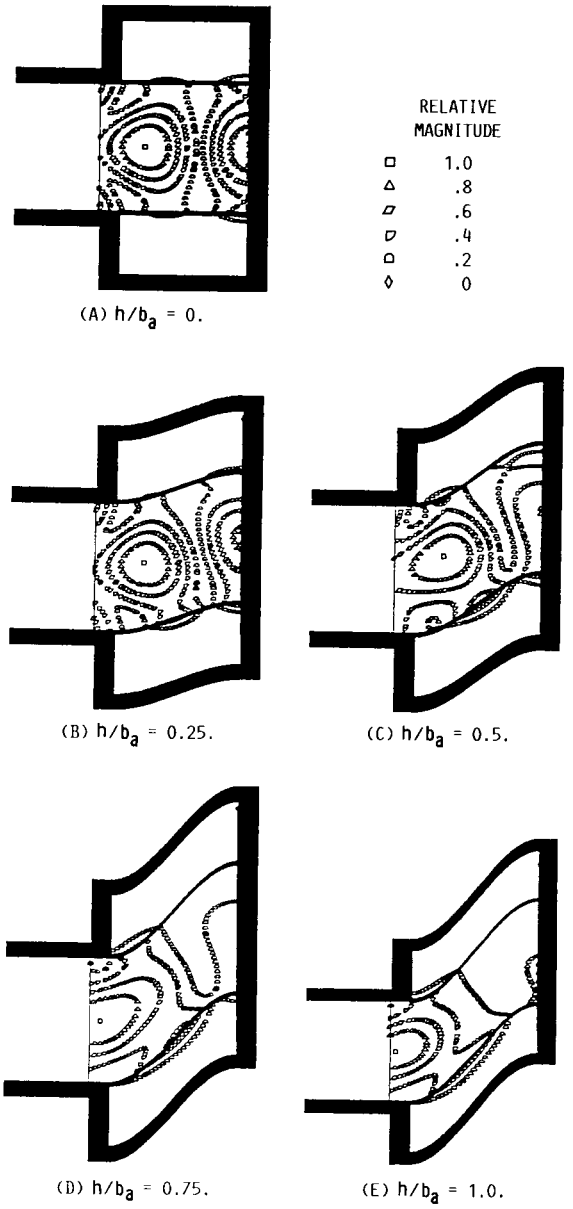

FIGURE 11. - EFFECT OF OFFSET OF ABSORBING WALL ON THE CONTOURS OF THE MAGNETIC FIELD WITH PEC EXIT CONDITION (L = 0.75, f = 1).

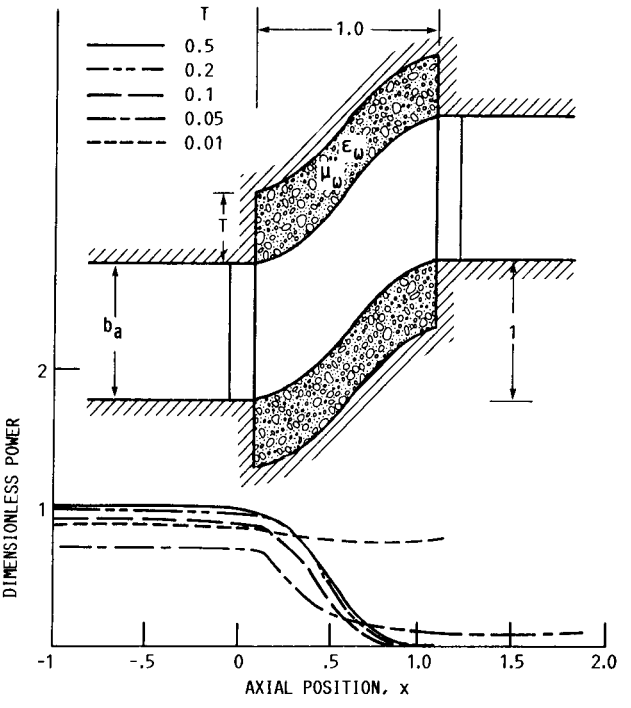

FIGURE 12. - EFFECT OF ABSORBER THICKNESS ON THE MAGNITUDE OF THE AXIAL POWER AS A FUNCTION OF POSITION (ε_ω = 1. - j2.83; μ_ω = 4.1).

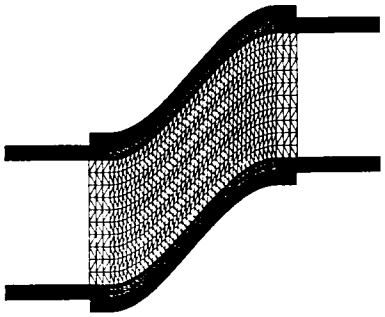

ΔX BASED ON WALL
PROPERTIES
$\varepsilon_\omega = 1.5\text{-}3.5j$
$\mu_\omega = 4.1$
ΔX = 0.02564

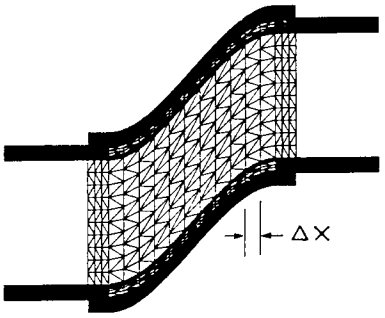

ΔX BASED ON AIR
PROPERTIES
$\varepsilon = 1$ $\mu = 1$
ΔX = 0.0909

(A) MODERATE CASE $= 1.5\text{-}3.5j$.

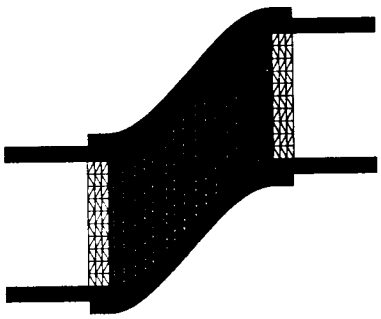

ΔX BASED ON WALL
PROPERTIES
$\varepsilon_\omega = 10.0\text{-}10.0j$
$\mu_\omega = 4.1$
ΔX = 0.0119

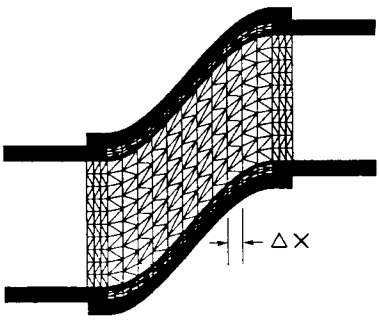

ΔX BASED ON AIR
PROPERTIES
$\varepsilon = 1$ $\mu = 1$
ΔX = 0.0909

(B) LARGE CASE $\varepsilon_\omega = 10.0\text{-}10.0j$.

FIGURE 13. - DISCRETIZATION OF AIR FILLED WAVE GUIDE WITH ABSORBERS MOUNTED ALONG BOTH UPPER AND LOWER WALLS.

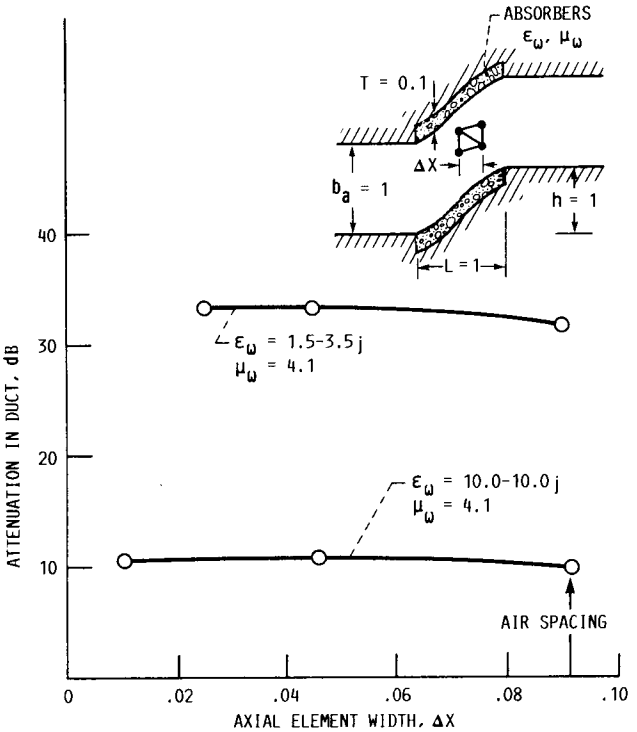

FIGURE 14. - ELECTROMAGNETIC ENERGY TRANSMISSION ATTENUATION AS A FUNCTION OF AXIAL NODE SPACING IN ABSORBER AND DUCT FOR CURVED DUCT (f = 1, L = 1, h = 1 WITH 5 VERTICAL NODES IN ABSORBER REGION).

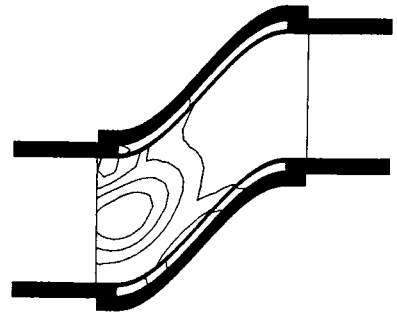

$\Delta X = 0.02564$
BASED ON WALL
PROPERTIES
$\varepsilon_\omega = 1.5\text{-}3.5j$
$\mu_\omega = 4.1$

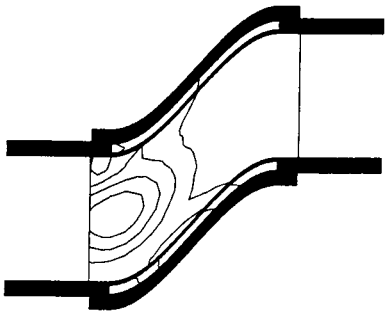

$\Delta X = 0.0909$
BASED ON AIR
PROPERTIES

(A) MODERATE CASE $\varepsilon_\omega = 1.5\text{-}3.5j$ $\mu_\omega = 4.1$.

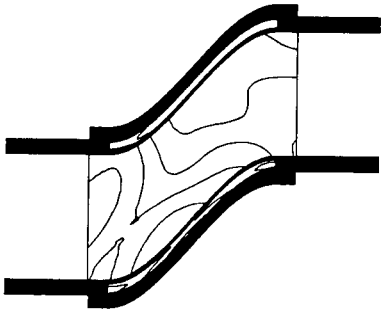

$\Delta X = 0.0119$
BASED ON WALL
PROPERTIES
$\varepsilon_\omega = 10.0\text{-}10.0j$
$\mu_\omega = 4.1$

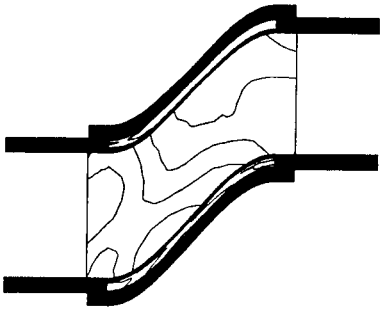

$\Delta X = 0.0909$
BASED ON AIR
PROPERTIES

(B) LARGE CASE $\varepsilon_\omega = 10.0\text{-}10.0j$ $\mu_\omega = 4.1$.

FIGURE 15. - CONTOUR PLOTS OF MAGNETIC FIELD AMPLITUDE.

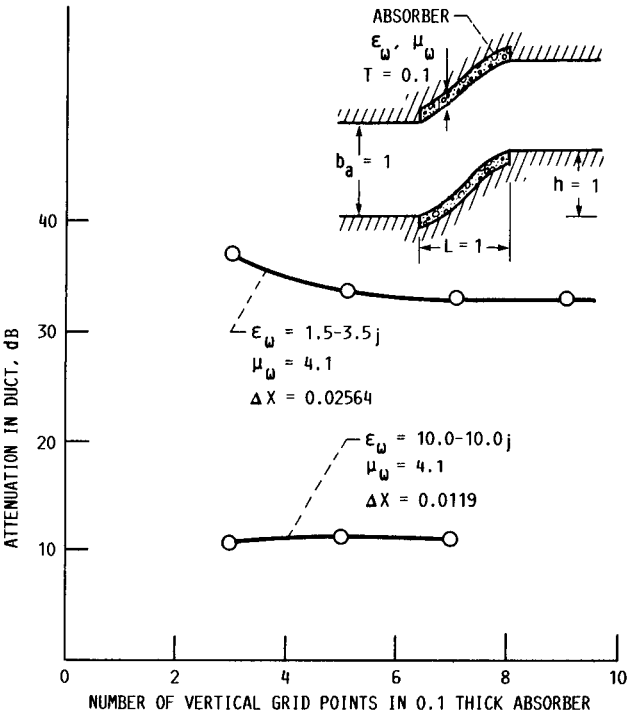

FIGURE 16. - ELECTROMAGNETIC ENERGY TRANSMISSION ATTENUATION AS A FUNCTION OF VERTICAL NODES IN ABSORBER FOR CURVED DUCT (f = 1, L = 1, h = 1).

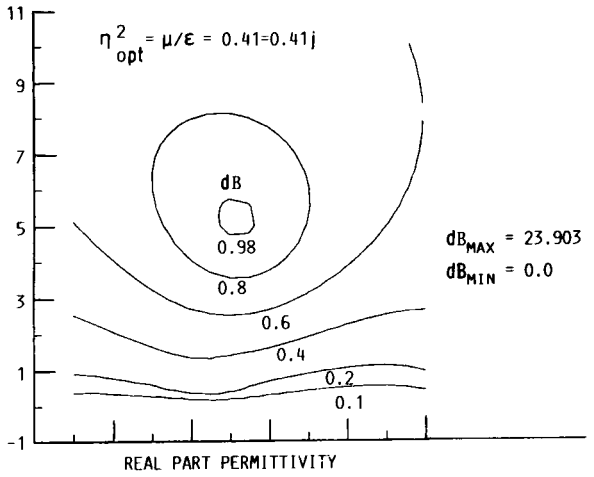

(A) INITIAL ITERATION - ε SEARCH ($\mu = 4.1$).

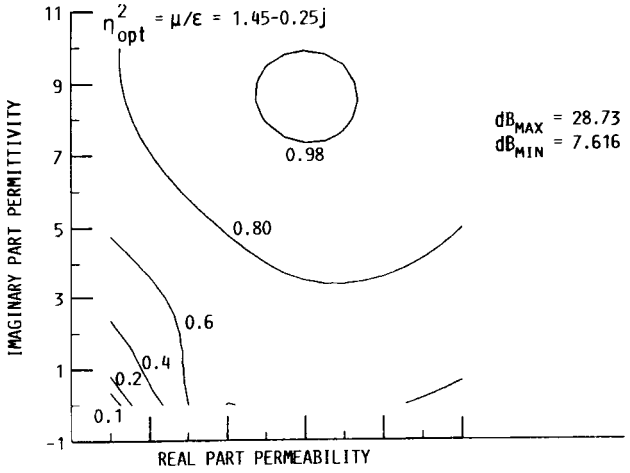

(B) SECOND ITERATION - μ SEARCH ($\varepsilon = 5.0-5.0j$).

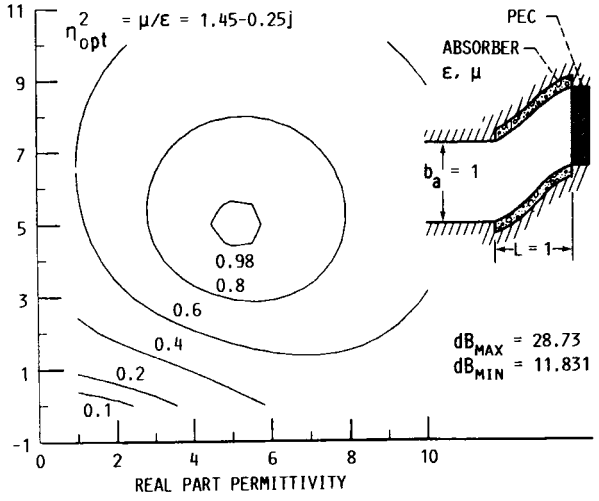

(C) THIRD ITERATION - ε SEARCH ($\mu = 6.0-8.5j$).

FIGURE 17. - ELECTROMAGNETIC REFLECTIVE ENERGY CONTOURS FOR CURVED DUCT WITH PEC EXIT ($f = 1$, $L = 1$, $h = 1$).

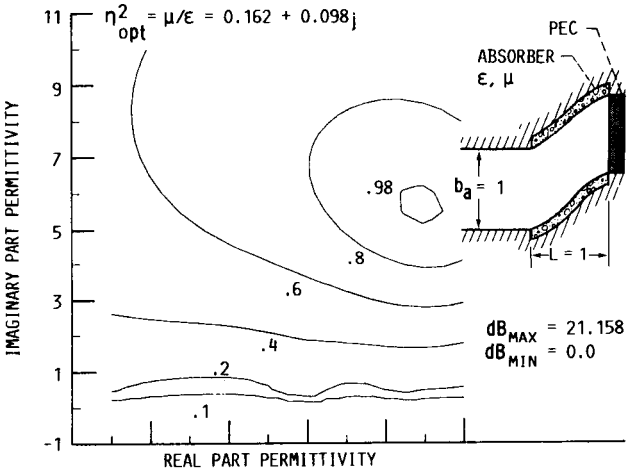

(A) INITIAL ITERATION - ε SEARCH ($\mu = 2.0$).

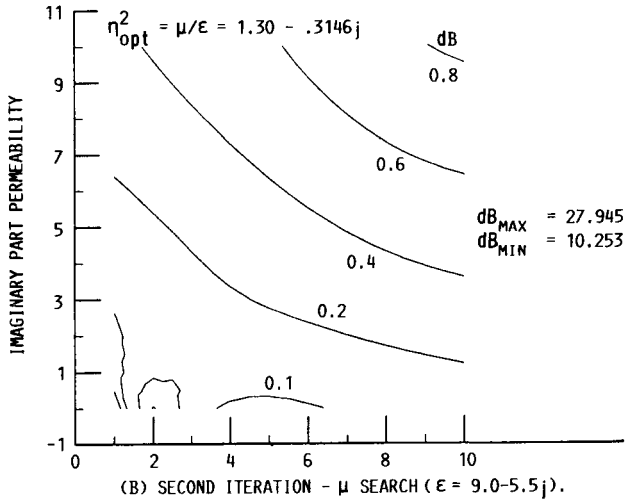

(B) SECOND ITERATION - μ SEARCH ($\varepsilon = 9.0-5.5j$).

FIGURE 18. - SENSITIVITY OF INITIAL STARTING POINT ON ELECTROMAGNETIC REFLECTIVE ENERGY CONTOURS FOR CURVED DUCT WITH PEC EXIT ($f = 1$, $L = 1$, $h = 1$).

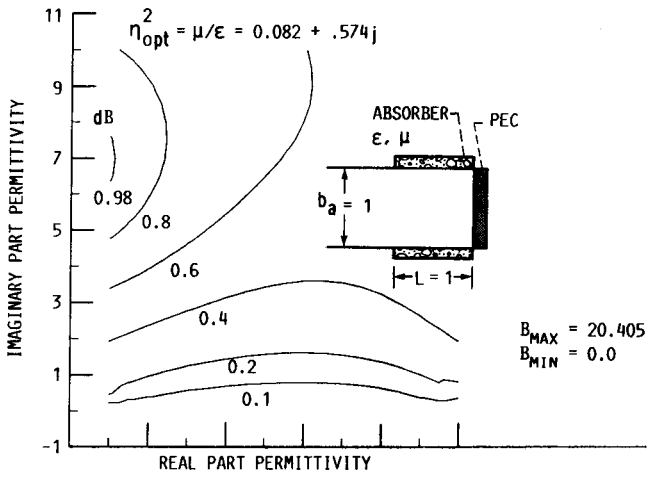

(A) INITIAL ITERATION - ε SEARCH. ($\mu = 4.1$).

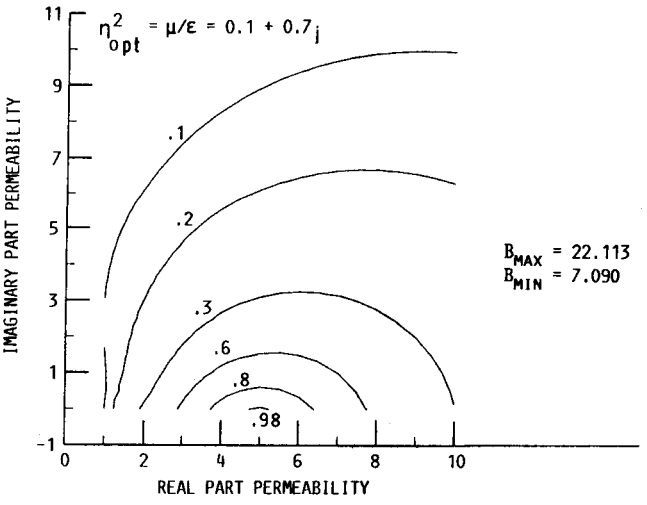

(B) SECOND ITERATION - μ SEARCH ($\epsilon = 1.0\text{-}7.0j$).

FIGURE 19. - ELECTROMAGNETIC REFLECTIVE ENERGY CONTOURS FOR STRAIGHT DUCT WITH PEC EXIT ($f = 1$, $L = 1$, $h = 0.0$).

NASA
National Aeronautics and Space Administration

Report Documentation Page

1. Report No.	2. Government Accession No.	3. Recipient's Catalog No.
NASA TM-102024		

4. Title and Subtitle	5. Report Date
Parametric Study of Electromagnetic Waves Propagating in Absorbing Curved S Ducts	July 1989
	6. Performing Organization Code

7. Author(s)	8. Performing Organization Report No.
Kenneth J. Baumeister	E-4761
	10. Work Unit No.
	505-62-21

9. Performing Organization Name and Address	11. Contract or Grant No.
National Aeronautics and Space Administration Lewis Research Center Cleveland, Ohio 44135-3191	
	13. Type of Report and Period Covered
	Technical Memorandum

12. Sponsoring Agency Name and Address	14. Sponsoring Agency Code
National Aeronautics and Space Administration Washington, D.C. 20546-0001	

15. Supplementary Notes

16. Abstract

A finite-element Galerkin formulation has been developed to study attenuation of transverse magnetic (TM) waves propagating in two-dimensional S-curved ducts with absorbing walls. In the frequency range where the duct diameter and electromagnetic wave length are nearly equal, the effect of duct length, curvature (duct offset), and absorber wall thickness was examined. For a given offset in the curved duct, the length of the S-duct was found to significantly affect both the absorptive and reflective characteristics of the duct. For a straight and a curved duct with perfect electric conductor terminations, power attenuation contours were examined to determine electromagnetic wall properties associated with maximum input signal absorption. Offset of the S-duct was found to significantly affect the value of the wall permittivity associated with the optimal attenuation of the incident electromagnetic wave.

17. Key Words (Suggested by Author(s))	18. Distribution Statement
Finite elements Electromagnetic waves Coatings	Unclassified – Unlimited Subject Category 32

19. Security Classif. (of this report)	20. Security Classif. (of this page)	21. No of pages	22. Price*
Unclassified	Unclassified	24	A03

NASA FORM 1626 OCT 86

*For sale by the National Technical Information Service, Springfield, Virginia 22161